Applied Physics Letters

Type-I band alignment at $MoS_2/In_{0.15}Al_{0.85}N$ lattice matched heterojunction and realization of MoS_2 quantum well

Cite as: Appl. Phys. Lett. **111**, 092104 (2017); https://doi.org/10.1063/1.4995976
Submitted: 13 July 2017 • Accepted: 17 August 2017 • Published Online: 31 August 2017

Malleswararao Tangi, Pawan Mishra, Ming-Yang Li, et al.

ARTICLES YOU MAY BE INTERESTED IN

Determination of band offsets at GaN/single-layer MoS_2 heterojunction
Applied Physics Letters **109**, 032104 (2016); https://doi.org/10.1063/1.4959254

Impact of N-plasma and Ga-irradiation on MoS_2 layer in molecular beam epitaxy
Applied Physics Letters **110**, 012101 (2017); https://doi.org/10.1063/1.4973371

Layer-transferred MoS_2/GaN PN diodes
Applied Physics Letters **107**, 103505 (2015); https://doi.org/10.1063/1.4930234

Lock-in Amplifiers up to 600 MHz

© 2017 Author(s).

AIP Publishing

Type-I band alignment at $MoS_2/In_{0.15}Al_{0.85}N$ lattice matched heterojunction and realization of MoS_2 quantum well

Malleswararao Tangi,[1,a)] Pawan Mishra,[1] Ming-Yang Li,[2] Mohammad Khaled Shakfa,[1] Dalaver H. Anjum,[3] Mohamed Nejib Hedhili,[3] Tien Khee Ng,[1,a)] Lain-Jong Li,[4,a)] and Boon S. Ooi[1,a)]

[1]*Photonics Laboratory, Computer, Electrical, and Mathematical Sciences and Engineering (CEMSE) Division, King Abdullah University of Science and Technology (KAUST), Thuwal 23955-6900, Saudi Arabia*
[2]*Research Center for Applied Sciences, Academia Sinica, Taipei 10617, Taiwan*
[3]*Imaging and Characterization Laboratory, King Abdullah University of Science and Technology (KAUST), Thuwal 23955-6900, Saudi Arabia*
[4]*Physical Science and Engineering (PSE) Division, King Abdullah University of Science and Technology (KAUST), Thuwal 23955-6900, Saudi Arabia*

(Received 13 July 2017; accepted 17 August 2017; published online 31 August 2017)

The valence and conduction band offsets (VBO and CBO) at the semiconductor heterojunction are crucial parameters to design the active region of contemporary electronic and optoelectronic devices. In this report, to study the band alignment parameters at the $In_{0.15}Al_{0.85}N/MoS_2$ lattice matched heterointerface, large area MoS_2 single layers are chemical vapor deposited on molecular beam epitaxial grown $In_{0.15}Al_{0.85}N$ films and vice versa. We grew InAlN having an in-plane lattice parameter closely matching with that of MoS_2. We confirm that the grown MoS_2 is a single layer from optical and structural analyses using micro-Raman spectroscopy and scanning transmission electron microscopy. The band offset parameters VBO and CBO at the $In_{0.15}Al_{0.85}N/MoS_2$ heterojunction are determined to be 2.08 ± 0.15 and 0.60 ± 0.15 eV, respectively, with type-I band alignment using high-resolution x-ray photoelectron spectroscopy in conjunction with ultraviolet photoelectron spectroscopy. Furthermore, we design a MoS_2 quantum well structure by growing an $In_{0.15}Al_{0.85}N$ layer on $MoS_2/In_{0.15}Al_{0.85}N$ type-I heterostructure. By reducing the nitrogen plasma power and flow rate for the overgrown $In_{0.15}Al_{0.85}N$ layers, we achieve unaltered structural properties and a reasonable preservation of photoluminescence intensity with a peak width of 70 meV for MoS_2 quantum well (QW). The investigation provides a pathway towards realizing large area, air-stable, lattice matched, and eventual high efficiency $In_{0.15}Al_{0.85}N/MoS_2/In_{0.15}Al_{0.85}N$ QW-based light emitting devices. © *2017 Author(s). All article content, except where otherwise noted, is licensed under a Creative Commons Attribution (CC BY) license (http://creativecommons.org/licenses/by/4.0/).* [http://dx.doi.org/10.1063/1.4995976]

Group III-V semiconductors have been extensively studied due to their potential applications in high efficiency electronic and optoelectronic devices such as high electron mobility transistors, light emitting diodes, and laser diodes.[1–4] Alongside, group VI transition metal dichalcogenides (TMDs) in the form of MX_2 have recently emerged as an atomic layered material system with promising electronic and optoelectronic properties.[5–8] Among the TMDs, molybdenum disulfide (MoS_2) in a single layer form is of potential interest for such devices owing to its direct bandgap and its prominent transport properties.[9,10] Recent advances in the integration of 2D-layered materials with wide band gap group-III nitride semiconductors are exciting due to their variety of applications in high current tunnel diodes.[11–13] In this context, several efforts were made to grow GaN on closely lattice matched TMDs. Yamada *et al.* reported the growth of GaN on bulk MoS_2 by plasma-enhanced molecular beam epitaxy (MBE).[14] Furthermore, there are a few reports on the growth of GaN on large area MoS_2 and WS_2 layers,[15,16] layered MoS_2 on GaN epilayers[17] by chemical vapor deposition (CVD) growth techniques, and layer transferred p-MoS_2 on GaN.[11] The band offset parameters (junction type: valence band offset—ΔE_v and conduction band offset—ΔE_c) are measured for various heterojunctions.[18–21] Recently, we have reported the growth of GaN on single layer (SL)-MoS_2 and SL-WSe_2 with type-II band alignment.[22,23]

In spite of the smaller in-plane lattice mismatch (≈0.8%) of GaN with MoS_2,[15] the type-II heterojunction formed by them can be solely utilized for electronic devices.[11–13] In contrast, optoelectronic devices formed by 2D/3D heterojunctions require a type-I band alignment which can be realized by using the group III-nitride alloys with higher bandgap as a constituent semiconducting layer of the 2D/3D heterojunction. Thus, $In_xAl_{1-x}N$ with a low In composition (12%–18%) exhibiting higher bandgap (>4.5 eV) and lattice matched to the MoS_2 layer with high contrast of the refractive index (≈30%) may be employed to achieve the type-I 2D/3D junction. Hence, the determination of the band offset parameters (VBO and CBO) and the type of junction for epitaxially formed $MoS_2/In_xAl_{1-x}N$ (or $In_xAl_{1-x}N/MoS_2$) heterointerfaces is necessary to provide a route towards the integration of group-III nitrides with TMDs for designing 2D/3D based optoelectronic devices. Furthermore, the

[a)]Authors to whom correspondence should be addressed: boon.ooi@kaust.edu.sa; lance.li@kaust.edu.sa; tienkhee.ng@kaust.edu.sa; and malleswara.tangi@kaust.edu.sa

 © Author(s) 2017.

introduction of nitrogen plasma quenches the photoluminescence intensity due to plasma-induced damage, and thus, a modified epitaxial process was utilized.

In this study, CVD grown SL-MoS_2 on Si and $In_{0.15}Al_{0.85}N$/Si and MBE grown $In_{0.15}Al_{0.85}N$ on Si and SL-MoS_2/Si and $In_{0.15}Al_{0.85}N$ epilayers were used to determine the band offsets at the $In_{0.15}Al_{0.85}N$/SL-MoS_2 heterointerface. Later, the structural and optical properties of the designed $In_{0.15}Al_{0.85}N/MoS_2/In_{0.15}Al_{0.85}N$ quantum well structure were studied.

The large area MoS_2 layers were prepared on Si(111) and $In_{0.15}Al_{0.85}N$/Si(111) substrates using a CVD system. The growth experiments of $In_{0.15}Al_{0.85}N$ on Si and MoS_2/Si substrates were carried out using the Veeco GEN 930 plasma-assisted molecular beam epitaxy (PAMBE) system at a substrate temperature of 500 °C. For $In_{0.15}Al_{0.85}N$ growth, the nitrogen plasma source was operated with a flow rate of 0.5 sccm and a radio frequency (RF) power of 200 W. In and Al metals were evaporated using a standard Knudsen cell with the beam equivalent pressure (BEP) values of $\approx 1 \times 10^{-8}$ and $\approx 4 \times 10^{-8}$ Torr. The crystallinity and composition of indium of the $In_xAl_{1-x}N$ epilayer were investigated using a CuK_α High-Resolution X-ray Diffractometer (HRXRD). High-angle annular dark field scanning transmission electron microscopy (HAADF-STEM) was utilized by operating a probe-corrected FEI Titan at an acceleration voltage of 300 kV. Using Horiba Aramis, room temperature (RT) Raman measurements were performed on $In_{0.15}Al_{0.85}N$ and MoS_2 layers with the excitation line of the He-Cd laser of 325 nm and the cobolt laser of 473 nm, respectively, whereas μPL emission was acquired on MoS_2/Si and $MoS_2/In_{0.15}Al_{0.85}N$ using a 473 nm excitation source. To probe the deep UV emission of $In_{0.15}Al_{0.85}N$, a Varian spectrometer with Xenon flash lamp as an excitation source was used. The high-resolution XPS measurements were carried out using a Kratos Axis Ultra DLD spectrometer equipped with a monochromatic Al K_α X-ray source ($h\nu = 1486.6$ eV). To acquire electron affinities of MoS_2 and $In_{0.15}Al_{0.85}N$, UPS measurements were performed using the He I ($h\nu_{He\text{-}I} = 21.2$ eV) photon source.

It is important to point out that the indium composition (x) can be chosen in such a way that the in-plane lattice mismatch between $In_xAl_{1-x}N$ and MoS_2 is vanishingly low (<0.5%). In order to accomplish such lattice matched $In_xAl_{1-x}N$ thin films, several kinetically controlled growth parameters were utilized having a prior idea of the growth conditions.[24] Figure 1(a) presents the HRXRD 2θ-ω scans obtained on the symmetric (on-axis) and asymmetric (off-axis) planes of the $In_xAl_{1-x}N$ film. Asymmetric planes were examined in skew symmetric geometry.[25] Figure 1(a) displays c-oriented peaks: InAlN(0002) at 35.28° along with the substrate Si(111) at 28.55° and Si(222) at 58.98° and the asymmetric reflection InAlN $(10\bar{1}1)$ at 37.13°. Using these on-axis and off-axis orientations of InAlN, the lattice parameters were extracted to be a = 0.3178 and c = 0.5087 nm. Thereby, the In composition was estimated to be ≈15% for epitaxially grown $In_xAl_{1-x}N$.[26] To inquire the surface morphology and root mean square (rms) roughness of InAlN/Si, atomic force microscopy scans were obtained in the tapping mode using an Agilent 5400 AFM. From Fig. 1(b), the root mean square (rms) surface roughness of the InAlN film is observed to be ≈1.5 nm. Figure 1(c) shows a nonlinear dependence of the bandgap of the $In_xAl_{1-x}N$ alloy on the In composition (X-axis) and the corresponding in-plane lattice parameter (alternate X axis). The inset of Fig. 1(c) shows the PL spectrum of the $In_xAl_{1-x}N$/Si sample exhibiting a peak position at ≈4.76 eV which is consistent with the estimated bandgap curve with the most accepted band bowing parameter b ≈ 5 eV.[27,28] As a result, we observe that the in-plane lattice parameter of $In_xAl_{1-x}N$ with an indium composition of 15% is well lattice matched with that of the MoS_2 layer.

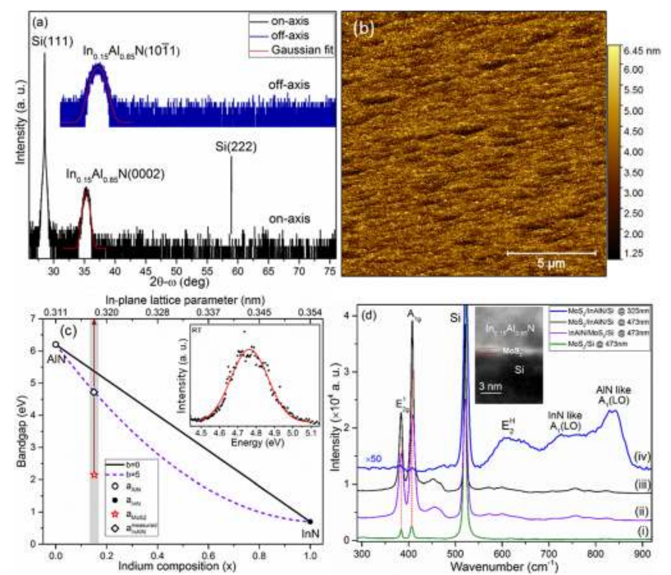

FIG. 1. (a) HRXRD 2θ-ω scans of on-axis and off-axis reflections acquired on the In_xAl_{1-x} N epilayer. (b) AFM surface morphology of the InAlN film. (c) Variation in the bandgap of the $In_xAl_{1-x}N$ alloy with the Indium composition for bowing parameters b = 0 and 5 eV and with the in-plane lattice parameter (alternate X-axis), and the corresponding inset shows the PL spectra of $In_{0.15}Al_{0.85}N$. (d) (i–iv) Micro-Raman spectra of MoS_2, $In_{0.15}Al_{0.85}N/MoS_2$ and $MoS_2/In_{0.15}Al_{0.85}N$. The respective inset shows a STEM cross-sectional image of the $In_{0.15}Al_{0.85}N/MoS_2$/Si heterojunction sample.

Micro-Raman spectroscopy was performed to investigate the optical quality and to ascertain the number of layers that accommodated in the CVD grown MoS_2 on Si and $In_{0.15}Al_{0.85}N$. Figure 1(d) (i–iii) shows the Raman spectra of MoS_2/Si, $In_{0.15}Al_{0.85}N/MoS_2$/Si, and $MoS_2/In_{0.15}Al_{0.85}N$/Si, which were obtained by employing a 473 nm laser. In order to obtain the enhanced Raman signal from $In_{0.15}Al_{0.85}N$ of the heterojunction, the measurements were carried out using 325 nm excitation by which the signal can overcome the reduced resonant excitation effect as shown in Fig. 1(d) (iv).[22,24] The two characteristic peaks in Fig. 1(d) observed at 385.5 ± 0.5 and $405.0 \pm 0.5\ cm^{-1}$ are attributed to E^1_{2g} and A_{1g} phonon modes of MoS_2, respectively. These modes correspond to the in-plane vibration of Mo and S atoms (E^1_{2g}) and out-of-plane vibration of S atoms (A_{1g}) in MoS_2. The separation between E^1_{2g} and A_{1g} phonon modes is found to be $19.5 \pm 0.5\ cm^{-1}$, which reveals that the MoS_2 layers deposited by CVD on Si and $In_{0.15}Al_{0.85}N$/Si templates are single layers.[29,30] The heterojunction $MoS_2/In_{0.15}Al_{0.85}N$ exhibits E^H_2, InN-like, and AlN-like A_1(LO) modes of $In_{0.15}Al_{0.85}N$ with the 325 nm excitation along with the extremely low intensity E^1_{2g} and A_{1g} modes of MoS_2. A two-mode behavior

of long wavelength optical phonons for $In_{0.15}Al_{0.85}N$ is due to the condition that either $m_{Al}<\mu_{(In,N)}$ or $m_{In}<\mu_{(Al,N)}$, where m is the mass and μ is the reduced mass.[31,32] In contrast, the phonon modes of $In_{0.15}Al_{0.85}N$ were not observed when the sample was excited with the 473 nm line, as shown in Fig. 1(d) (ii and iii), which is ascribed to the reduced resonant excitation effect.[22] Moreover, as a consequence of this resonant effect, in Fig. 1(d) (iv), the intensity of E^1_{2g} and A_{1g} of MoS_2 observed to be extremely lower than E^H_2, InN-like, and AlN-like A_1(LO) phonon modes of $In_{0.15}Al_{0.85}N$ with 325 nm excitation. Thus, these results show the sustainability of the MoS_2 layer during the growth of $In_{0.15}Al_{0.85}N$. The inset of Fig. 1(d) shows the cross-sectional STEM image acquired at the $In_{0.15}Al_{0.85}N$/SL-MoS_2/Si heterojunction having a MoS_2 layer thickness of ≈0.8 nm, which is in good agreement with the thickness of the S-Mo-S single-layer.[33] Thus, micro-Raman and STEM measurements confirm that the SL-MoS_2 is epitaxially grown on the lattice matched $In_{0.15}Al_{0.85}N$ films and vice versa.

High-resolution XPS measurements were extensively employed to determine the valence band offset (VBO) of a heterointerface. To evaluate VBO at the $MoS_2/In_{0.15}Al_{0.85}N$ interface, the energy difference between the Mo and In core levels from the $MoS_2/In_{0.15}Al_{0.85}N$ ($In_{0.15}Al_{0.85}N/MoS_2$) heterojunction sample and the energy of core levels relative to the respective valence band maximum (VBM) of the MoS_2 and $In_{0.15}Al_{0.85}N$ samples are required to be evaluated. Since the escape depth of photo-emitted electrons in HRXPS is significantly low, the overgrown MoS_2 ($In_{0.15}Al_{0.85}N$) layer of heterojunction sample $MoS_2/In_{0.15}Al_{0.85}N$ ($In_{0.15}Al_{0.85}N/MoS_2$) has to be thin enough so that the electrons removed from both thin overgrown MoS_2 ($In_{0.15}Al_{0.85}N$) and underlying $In_{0.15}Al_{0.85}N$ (MoS_2) layers can be easily probed.[34] Furthermore, the surface area of MoS_2 is sufficiently large to carry out the XPS measurements. In particular, due to the non-continuity of the MoS_2 layer on Si and $In_{0.15}Al_{0.85}N$ templates, the region of interest on MoS_2/Si and $MoS_2/In_{0.15}Al_{0.85}N$ samples was selectively chosen within the spatial resolution of HRXPS.[21,35] This was executed by comparing the intensity of Mo 3d and In 3d and Si 2p core-levels, which allowed us to collect the photoemission signal solely from MoS_2/Si and $MoS_2/In_{0.15}Al_{0.85}N$ ($In_{0.15}Al_{0.85}N/MoS_2$), respectively. To determine the VBO, the core levels Mo 3d and In 3d were used for the analysis. The VBO for the $MoS_2/In_{0.15}Al_{0.85}N$ heterojunction can be calculated by the method provided by Kraut *et al.*,[36] which is expressed as

$$\Delta E_v = \left(E^{MoS_2}_{Mo3d_{5/2}} - E^{MoS_2}_{VBM}\right) + \left(E^{MoS_2/InAlN}_{In3d_{5/2}} - E^{MoS_2/InAlN}_{Mo3d_{5/2}}\right) - \left(E^{InAlN}_{In3d_{5/2}} - E^{InAlN}_{VBM}\right). \quad (1)$$

From Fig. 2(a), the first term of Eq. (1) deduced by taking into account the position of the Mo $3d_{5/2}$ core-level referenced with respect to the VBM, which is measured to be 228.88 ± 0.15 eV. The valence band maxima (VBM) values are determined by extrapolating the linear leading edge of the valence band to the base level.[37,38] In the peak deconvolution process, Voigt (mixed Lorentzian-Gaussian) line shapes were employed for fitting the Mo-S, S-Mo (trigonal prismatic,

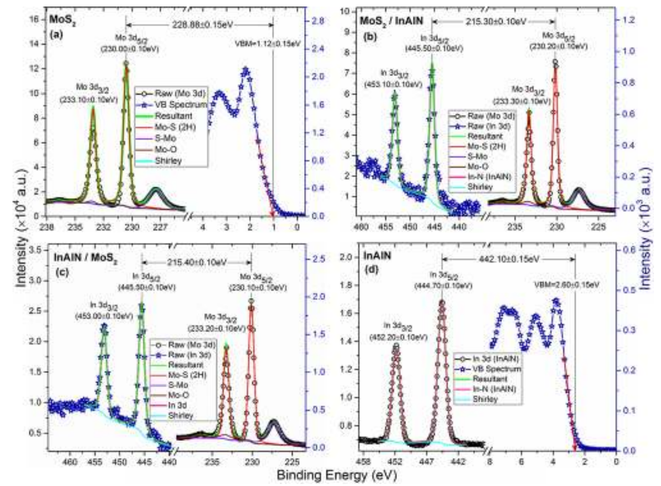

FIG. 2. (a) The Mo 3d core-level and valence band spectra collected on SL-MoS_2, representing the binding energy separation between the Mo $3d_{5/2}$ corelevel and VBM. (b) and (c) The spectra of In 3d and Mo 3d core-levels acquired on SL-$MoS_2/In_{0.15}Al_{0.85}N$ and $In_{0.15}Al_{0.85}N$/SL-MoS_2 heterojunction samples. (d) In 3d core-level and valence band spectra obtained for the $In_{0.15}Al_{0.85}N$ epilayer, providing the binding energy difference between In $3d_{5/2}$ and VBM. The peak positions of core-levels are shown in parentheses.

-2 H), and M-O chemical states, respectively, centered at 230.00 ± 0.10, 227.50 ± 0.10, and 233.00 ± 0.10 eV, respectively. The Mo-O state with extremely low intensity results from the MoO_3 precursor at the interface of MoS_2/Si during the high temperature CVD growth process. In order to evaluate the subsequent term in Eq. (1), $MoS_2/In_{0.15}Al_{0.85}N$ and $In_{0.15}Al_{0.85}N/MoS_2$ samples were used for XPS measurements where we consider the difference between In $3d_{5/2}$ and Mo $3d_{5/2}$ core-levels as described in Figs. 2(b) and 2(c). Here, the In 3d core-level is deconvoluted with the In-N bonding, and no other states are observed. Figure 2(b) shows the fitting of the Mo 3d core-level equipped with three chemical states as similar to the states in the Mo 3d core-level of MoS_2 in Fig. 2(a). Thereby, the binding energy separation between Mo $3d_{5/2}$ and In $3d_{5/2}$ core-levels for $MoS_2/In_{0.15}Al_{0.85}N$ is found to be 215.30 ± 0.10 eV, which is well corroborated with that of the $In_{0.15}Al_{0.85}N/MoS_2$ heterojunction (215.40 ± 0.10 eV) as shown in Fig. 2(c). The $3d_{3/2}$ core-levels of Mo and In have similar deconvolutions at higher binding energy values differed by ≈3.10 and ≈7.50 eV, respectively, from Mo $3d_{5/2}$ and In $3d_{5/2}$ states. The deconvolution of the Mo 3d core-level for the heterojunction sample infers the absence of the octahedral phase in MoS_2 which is in contrast to the previous report[22] due to the low flow rate and radiofrequency (RF) power of the nitrogen plasma source used for the growth of the $In_{0.15}Al_{0.85}N$ sample. Thus, the structural properties of MoS_2 layers of the heterojunction remain unaltered. The Mo-S bonding peak infers the sustainability of MoS_2 at $In_{0.15}Al_{0.85}N$ growth temperature in the UHV oxygen free environment. The absence of any other chemical states associated with Mo or S bonding in the In 3d core-level spectrum is a clear evidence of Vander Waal epitaxy. The last term of Eq. (1) indicates the binding energy difference of 442.10 ± 0.10 eV measured between the In $3d_{5/2}$ core level of 444.70 ± 0.10 eV and the respective VBM of 2.60 ± 0.15 eV as shown in Fig. 2(d). The In $3d_{5/2}$ and $3d_{3/2}$ core-levels are deconvoluted with the In-N bonding states at

444.70 ± 0.10 and 452.20 ± 0.10 eV, respectively. The Fermi level position with respect to the VBM as shown in Figs. 2(a) and 2(d) infers that $In_{0.15}Al_{0.85}N$ and MoS_2 layers are nearly intrinsic materials. Thus, the VBO is determined from Eq. (1) to be ≈2.08 ± 0.15 eV.

The substitution of VBO (ΔE_v) obtained from HRXPS analysis as described in Fig. 2 and electronic bandgap values of MoS_2 ($E_g^{MoS_2} = 2.15$ eV)[21] and $In_{0.15}Al_{0.85}N$ ($E_g^{InAlN} = 4.83$ eV) epilayers in the following equation allow us to extract the conduction band offset (CBO) ΔE_c of the $MoS_2/In_{0.15}Al_{0.85}N$ heterostructure.

$$\Delta E_c = E_g^{InAlN} - \Delta E_v - E_g^{MoS_2}. \tag{2}$$

Thus, from Eq. (2), the CBO (ΔE_c) is determined to be 0.60 ± 0.15 eV. Furthermore, the measured CBO value is verified by Anderson's affinity rule which is defined as the difference between the electron affinity values of constituent semiconductors of the heterojunction.[39] In order to verify the CBO by employing the affinity rule to the $MoS_2/In_{0.15}Al_{0.85}N$ interface, the electron affinities of constituent materials are required. UPS measurements were performed on MoS_2/Si and $In_{0.15}Al_{0.85}N$/Si to determine the electron affinity of constituent materials of the heterojunction. Figures 3(a) and 3(b) show the UPS spectra recorded on MoS_2/Si and $In_{0.15}Al_{0.85}N$/Si. The electron affinities were measured using the following equation:

$$\chi = h\nu_{He-I} - \Omega - E_g, \tag{3}$$

where $h\nu_{He-I}$ is the photon energy of the He-I line, Ω is the spectrum width, and E_g is the electronic band gap. The spectrum width (Ω) is the energy separation between the VBM and cutoff energy of secondary electrons with a sharp photoemission onset as shown in Figs. 3(a) and 3(b) for MoS_2 and $In_{0.15}Al_{0.85}N$, respectively. Fermi level positions obtained from UPS are slightly shifted to higher binding energy than that of HRXPS, as the charging induced shifts are not corrected in UPS spectra. Thus, the electron affinity, energy separation between the vacuum level and CBM, values were determined to be 4.10 ± 0.10 and 3.50 ± 0.10 eV for MoS_2 and $In_{0.15}$ $Al_{0.85}N$ using Eq. (3). Hence, from Anderson's affinity rule, the obtained CBO for the $MoS_2/In_{0.15}Al_{0.85}N$ heterojunction from UPS analysis is 0.60 ± 0.10 eV, which is

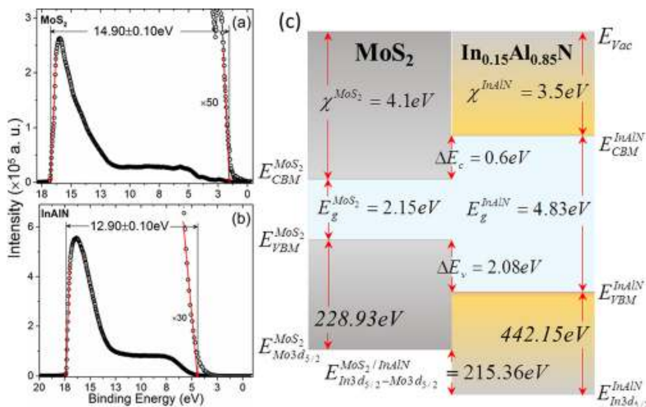

FIG. 3. (a) and (b) Ultraviolet photoelectron spectroscopy (UPS) scans for MoS_2 and $In_{0.15}Al_{0.85}N$ samples. (c) Schematic representation of the type I band alignment at the $MoS_2/In_{0.15}Al_{0.85}N$ heterojunction.

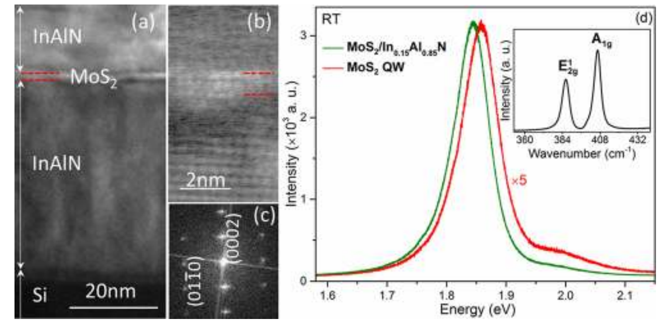

FIG. 4. (a) and (b) Low and high magnification cross-sectional images of high-angle annular dark field-scanning transmission electron microscopy (HAADF-STEM) for the MoS_2 QW sample. (c) FFT image obtained for $In_{0.15}Al_{0.85}N$ barrier layers. (d) μPL spectra of $MoS_2/In_{0.15}Al_{0.85}N$ and MoS_2 QW, and the inset shows the Raman spectra of the MoS_2 QW.

in good agreement with the CBO value determined from HRXPS studies. Thus, obtained CBO and VBO facilitate the determination of the type of band alignment at the heterojunction. Thereby, the experimentally measured offset parameters from this study are represented as a schematic of the band alignment diagram in Fig. 3(c) which pertains to the type-I heterostructure.

Figure 4(a) shows the cross sectional high-angle annular dark field-scanning transmission electron microscopy (HAADF-STEM) image recorded across the stack of $In_{0.15}Al_{0.85}N/MoS_2/In_{0.15}Al_{0.85}N$ layers which were prepared by FIB. This reveals that the thickness of the MoS_2 well layer is ≈0.85 nm, while the thickness values of the top and bottom barrier layers are of ≈10 and ≈40 nm, respectively. Figure 4(b) shows the magnified STEM image of (a). Figure 4(c) displays the FFT image acquired on the $In_{0.15}Al_{0.85}N$ barrier layer, which shows the wurtzite crystal structure with a c-oriented growth corroborated by the HRXRD measurements. Thus, the HAADF-STEM analysis is a clear evidence of the formation of a single layer MoS_2 QW sandwiched between $In_{0.15}Al_{0.85}N$ layers. Furthermore, the free exciton peak at ≈1.87 in μPL spectra as shown in Fig. 4(d) for the MoS_2 QW is slightly blue shifted with respect to the PL peak at 1.84 eV of $MoS_2/In_{0.15}Al_{0.85}N$. Here, we compare PL spectra of $MoS_2/In_{0.15}Al_{0.85}N$ and MoS_2 QWs to rule out the peak shifts associated with the strain. Thus, the blue shift of ≈30 meV is attributed to the quantum size induced confinement effect. This observed blue shift is far less than the reported blue shift for MoS_2 QDs,[40] which can be due to the van der Waals epitaxy with reduced confinement effects in the QW structure. The peaks at 1.87 and ≈2.03 eV are the exciton resonances corresponding to the transitions from the conduction band to two spin-split valence sub-bands that originated from the broken inversion symmetry of the crystal lattice.[41,42] The low intensity of PL for the QW is ascribed to the non-resonant excitation, which means that the $In_{0.15}Al_{0.85}N$ barrier layers are not excited along with the MoS_2 QW.[43] However, our previous reports show the enormous quenching (100–150 times) of PL for nitrogen plasma irradiated MoS_2 layers and 2D/3D heterojunctions.[16,23] In this study, we preserved the PL signal of the QW with relatively high intensity (quenched by 5 times) and a comparable peak width of 70 meV by using the low nitrogen flow rate and low forward power of plasma source for the growth of $In_{0.15}Al_{0.85}N$ barrier

layers. The respective inset shows the Raman spectra for the QW sample having the phonon mode separation of $19.5 \pm 0.5\,cm^{-1}$, which clarifies that the MoS_2 QW is a single layer.

In conclusion, MoS_2 single layers were chemical vapor deposited on the PAMBE grown $In_{0.15}Al_{0.85}N$ template to study the band alignment at the lattice matched $MoS_2/In_{0.15}Al_{0.85}N$ heterointerface. We confirm that the CVD deposited MoS_2 is a single layer by means of micro-Raman phonon modes and STEM. The determination of band offset parameters at the $MoS_2/In_{0.15}Al_{0.85}N$ heterostructure was carried out by utilizing the HRXPS and UPS measurements. We determine the valence band and conduction band offset values of 2.08 ± 0.15 eV and 0.6 ± 0.15 eV, respectively, with type-I band alignment at the $MoS_2/In_{0.15}Al_{0.85}N$ heterostructure. Furthermore, we prepared a MoS_2 QW by growing the $In_{0.15}Al_{0.85}N$ top barrier layer on the $MoS_2/In_{0.15}Al_{0.85}N$ template. The blue shift in PL spectra with respect to the MoS_2 single layer confirmed that the MoS_2 well exhibits the quantum confinement effect. The PL properties of the QW were preserved with a peak width of 70 meV by lowering the nitrogen plasma power and N_2 flow rate of overgrown $In_{0.15}Al_{0.85}N$ layers. Therefore, our investigation indicated a feasible route for large area integration of 3D group III nitride materials with 2D transition metal dichalcogenide layers for future high efficiency, air-stable, and reliable applications of 2D/3D based photonic and optoelectronic applications.

We acknowledge the financial support from King Abdulaziz City for Science and Technology (KACST), Grant No. KACST TIC R2-FP-008, and baseline funding BAS/1/1614-01-01 of the King Abdullah University of Science and Technology (KAUST).

[1]S. Nakamura, Science **281**, 956 (1998).
[2]L. Shen, S. Heikman, B. Moran, R. Coffie, N.-Q. Zhang, D. Buttari, I. P. Smorchkova, S. Keller, S. P. DenBaars, and U. K. Mishra, IEEE Electron Device Lett. **22**, 457 (2001).
[3]Y. Sun, K. Zhou, Q. Sun, J. Liu, M. Feng, Z. Li, Y. Zhou, L. Zhang, D. Li, S. Zhang, M. Ikeda, S. Liu, and H. Yang, Nat. Photonics **10**, 595 (2016).
[4]D. Saxena, S. Mokkapati, P. Parkinson, N. Jiang, Q. Gao, H. H. Tan, and C. Jagadish, Nat. Photonics **7**, 963 (2013).
[5]B. Radisavljevic, A. Radenovic, J. Brivio, V. Giacometti, and A. Kis, Nat. Nanotechnol. **6**, 147 (2011).
[6]B. W. H. Baugher, H. O. H. Churchill, Y. Yang, and P. Jarillo-Herrero, Nat. Nanotechnol. **9**, 262 (2014).
[7]J. Pu, K. Kanahashi, N. T. Cuong, C.-H. Chen, L.-J. Li, S. Okada, H. Ohta, and T. Takenobu, Phys. Rev. B **94**, 14312 (2016).
[8]M.-Y. Li, Y. Shi, C.-C. Cheng, L.-S. Lu, Y.-C. Lin, H.-L. Tang, M.-L. Tsai, C.-W. Chu, K.-H. Wei, J.-H. He, W.-H. Chang, K. Suenaga, and L.-J. Li, Science **349**, 524 (2015).
[9]C. Zhang, A. Johnson, C. L. Hsu, L. J. Li, and C. K. Shih, Nano Lett. **14**, 2443 (2014).
[10]B. W. H. Baugher, H. O. H. Churchill, Y. Yang, and P. Jarillo-Herrero, Nano Lett. **13**, 4212 (2013).
[11]E. W. Lee II, C. H. Lee, P. K. Paul, L. Ma, W. D. McCulloch, S. Krishnamoorthy, Y. Wu, A. R. Arehart, and S. Rajan, Appl. Phys. Lett. **107**, 103505 (2015).
[12]S. Krishnamoorthy, E. W. Lee, C. H. Lee, Y. Zhang, W. D. McCulloch, J. M. Johnson, J. Hwang, Y. Wu, and S. Rajan, Appl. Phys. Lett. **109**(18), 183505 (2016).
[13]A. Zubair, A. Nourbakhsh, J.-Y. Hong, M. Qi, Y. Song, D. Jena, J. Kong, M. Dresselhaus, and T. Palacios, Nano Lett. **17**, 3089 (2017).
[14]A. Yamada, K. P. Ho, T. Maruyama, and K. Akimoto, Appl. Phys. A Mater. Sci. Process. **69**, 89 (1999).
[15]P. Gupta, A. A. Rahman, S. Subramanian, S. Gupta, A. Thamizhavel, T. Orlova, S. Rouvimov, S. Vishwanath, V. Protasenko, M. R. Laskar, H. G. Xing, D. Jena, and A. Bhattacharya, Sci. Rep. **6**, 23708 (2016).
[16]P. Mishra, M. Tangi, T. K. Ng, M. N. Hedhili, D. H. Anjum, M. S. Alias, C.-C. Tseng, L.-J. Li, and B. S. Ooi, Appl. Phys. Lett. **110**, 12101 (2017).
[17]D. Ruzmetov, K. Zhang, G. Stan, B. Kalanyan, G. R. Bhimanapati, S. M. Eichfeld, R. A. Burke, P. B. Shah, T. P. O'Regan, F. J. Crowne, A. G. Birdwell, J. A. Robinson, A. V. Davydov, and T. G. Ivanov, ACS Nano **10**, 3580 (2016).
[18]P. D. C. King, T. D. Veal, C. Kendrick, L. Bailey, S. Durbin, and C. F. McConville, Phys. Rev. B **78**, 33308 (2008).
[19]G. Martin, S. Strite, A. Botchkarev, A. Agarwal, A. Rockett, H. Morkoç, W. R. L. Lambrecht, and B. Segall, Appl. Phys. Lett. **65**, 610 (1994).
[20]T. N. Bhat, M. Kumar, M. K. Rajpalke, B. Roul, S. B. Krupanidhi, and N. Sinha, J. Appl. Phys. **109**, 123707 (2011).
[21]M.-H. Chiu, C. Zhang, H.-W. Shiu, C.-P. Chuu, C.-H. Chen, C.-Y. S. Chang, C.-H. Chen, M.-Y. Chou, C.-K. Shih, and L.-J. Li, Nat. Commun. **6**, 7666 (2015).
[22]M. Tangi, P. Mishra, T. K. Ng, M. N. Hedhili, B. Janjua, M. S. Alias, D. H. Anjum, C. C. Tseng, Y. Shi, H. J. Joyce, L. J. Li, and B. S. Ooi, Appl. Phys. Lett. **109**, 32104 (2016).
[23]M. Tangi, P. Mishra, C.-C. Tseng, T. K. Ng, M. N. Hedhili, D. H. Anjum, M. S. Alias, N. Wei, L.-J. Li, and B. S. Ooi, ACS Appl. Mater. Interfaces **9**, 9110 (2017).
[24]M. Tangi, P. Mishra, B. Janjua, T. K. Ng, D. H. Anjum, A. Prabaswara, Y. Yang, A. M. Albadri, A. Y. Alyamani, M. M. El-Desouki, and B. S. Ooi, J. Appl. Phys. **120**, 45701 (2016).
[25]M. Tangi, A. De, J. Ghatak, and S. M. Shivaprasad, J. Appl. Phys. **119**, 205701 (2016).
[26]V. Darakchieva, M. Beckers, M. Y. Xie, L. Hultman, B. Monemar, J. F. Carlin, E. Feltin, M. Gonschorek, and N. Grandjean, J. Appl. Phys. **103**, 103513 (2008).
[27]W. Terashima, S.-B. Che, Y. Ishitani, and A. Yoshikawa, Jpn. J. Appl. Phys., Part 2 **45**, L539 (2006).
[28]T. S. Oh, J. O. Kim, H. Jeong, Y. S. Lee, S. Nagarajan, K. Y. Lim, C.-H. Hong, and E.-K. Suh, J. Phys. D. Appl. Phys. **41**, 95402 (2008).
[29]J. Huang, L. Yang, D. Liu, J. Chen, Q. Fu, Y. Xiong, F. Lin, and B. Xiang, Nanoscale **7**, 4193 (2015).
[30]C. Lee, H. Yan, L. E. Brus, T. F. Heinz, J. Hone, and S. Ryu, ACS Nano **4**, 2695 (2010).
[31]T.-T. Kang, A. Hashimoto, and A. Yamamoto, Phys. Rev. B **79**, 33301 (2009).
[32]I. F. Chang and S. S. Mitra, Phys. Rev. **172**, 924 (1968).
[33]Y. H. Lee, X. Q. Zhang, W. Zhang, M. T. Chang, C. Te Lin, K. D. Chang, Y. C. Yu, J. T. W. Wang, C. S. Chang, L. J. Li, and T. W. Lin, Adv. Mater. **24**, 2320 (2012).
[34]C. S. Fadley, Surf. Interface Anal. **40**, 1579 (2008).
[35]J. Choi, H. Zhang, and J. H. Choi, ACS Nano **10**, 1671 (2016).
[36]E. A. Kraut, R. W. Grant, J. R. Waldrop, and S. P. Kowalczyk, Phys. Rev. Lett. **44**, 1620 (1980).
[37]S. W. King, C. Ronning, R. F. Davis, M. C. Benjamin, and R. J. Nemanich, J. Appl. Phys. **84**, 2086 (1998).
[38]M. Tangi, J. Kuyyalil, and S. M. Shivaprasad, J. Appl. Phys. **114**, 153501 (2013).
[39]R. L. Anderson, IBM J. Res. Dev. **4**, 283 (1960).
[40]S. Mukherjee, R. Maiti, A. K. Katiyar, S. Das, and S. K. Ray, Sci. Rep. **6**, 29016 (2016).
[41]W. Jin, P. C. Yeh, N. Zaki, D. Zhang, J. T. Sadowski, A. Al-Mahboob, A. M. Van Der Zande, D. A. Chenet, J. I. Dadap, I. P. Herman, P. Sutter, J. Hone, and R. M. Osgood, Phys. Rev. Lett. **111**, 106801 (2013).
[42]G. Eda, H. Yamaguchi, D. Voiry, T. Fujita, M. Chen, and M. Chhowalla, Nano Lett. **11**, 5111 (2011).
[43]Y. Fang, L. Wang, Q. Sun, T. Lu, Z. Deng, Z. Ma, Y. Jiang, H. Jia, W. Wang, J. Zhou, and H. Chen, Sci. Rep. **5**, 12718 (2015).